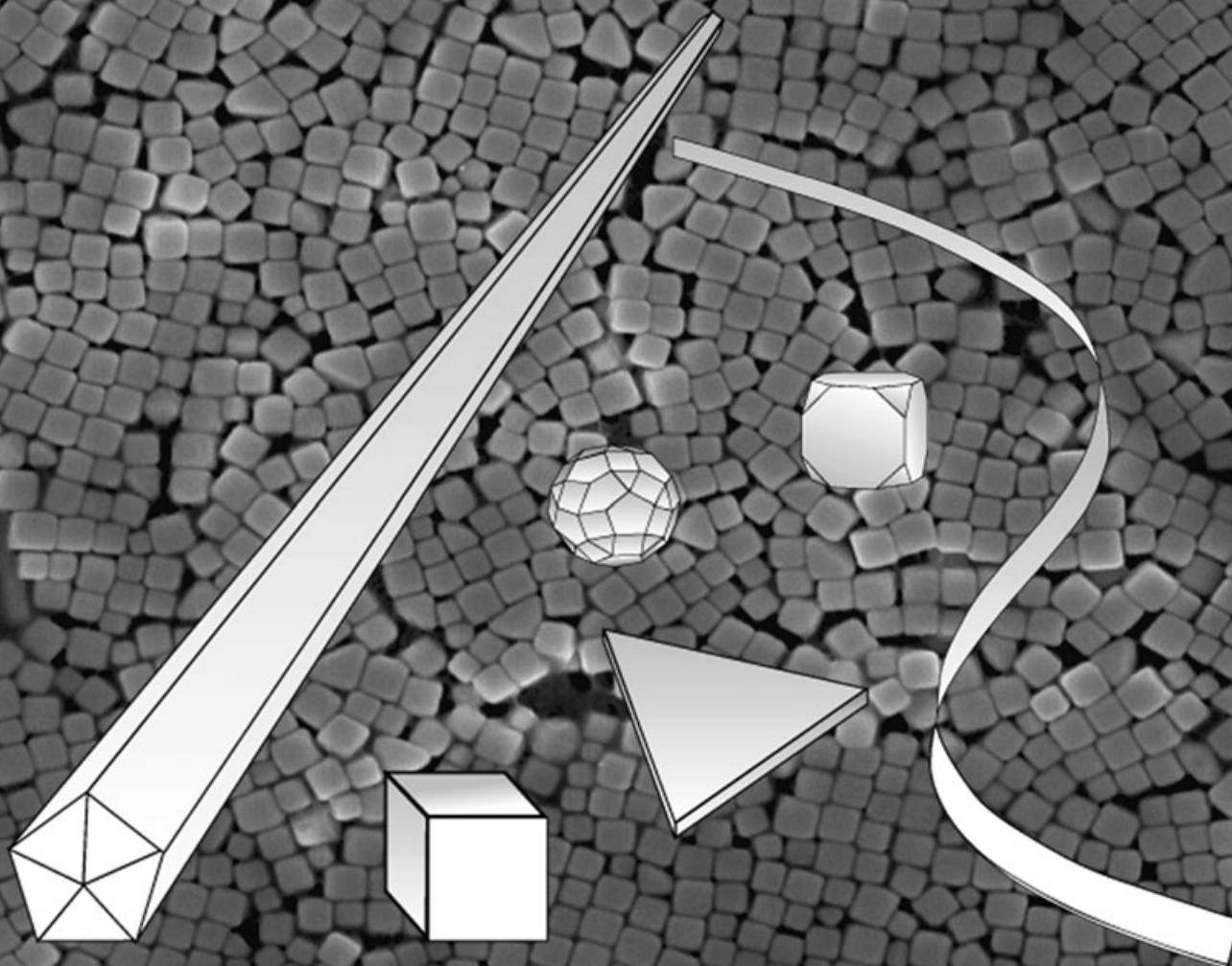


Shape Control of



Silver Nanoparticles

Shape-Controlled Synthesis of Metal Nanostructures: The Case of Silver

Benjamin Wiley⁺, Yugang Sun⁺, Brian Mayers, and Younan Xia^{*[a]}

Abstract: The concept of shape-controlled synthesis is discussed by investigating the growth mechanisms for silver nanocubes, nanowires, and nanospheres produced through a polymer-mediated polyol process. Experimental parameters, such as the concentration of AgNO₃ (the precursor to silver), the molar ratio between poly(vinylpyrrolidone) (PVP, the capping agent) and AgNO₃, and the strength of chemical interaction between PVP and various crystallographic planes of silver, were found to determine the crystallinity of seeds (e.g., single crystal versus decahedral multiply twinned particles). In turn, the crystallinity of a seed and the extent of the PVP coverage on the seed were both instrumental in controlling the morphology of final product. The ability to generate silver nanostructures with well-defined morphologies provides a great opportunity to experimentally and systematically study the relationship between their properties and geometric shapes.

Keywords: nanostructures • polymers • shape-controlled synthesis • silver

Introduction

Synthesis of metal nanostructures has been an active research area for many decades, because of the importance of these materials to catalysis, photography, electronics, photonics, information storage, optoelectronics, biological labeling, imaging, and sensing.^[1] Like their semiconductor cousins (e.g., quantum dots), the intrinsic properties of metal nanostructures can be tailored by controlling their size,

shape, composition, crystallinity, and structure (e.g., solid versus hollow).^[2] Particular emphasis has recently been placed on the control of shape, because in many cases it allows one to fine tune the properties with a greater versatility than can be achieved otherwise. For example, computational work has predicted that, for silver or gold nanoparticles, the number and position of surface plasmon resonance (SPR) peaks, as well as the effective spectral range for surface-enhanced Raman scattering (SERS), are strongly dependent on the particle shape.^[3] Experimentally, the longitudinal SPR modes of silver and gold nanorods have been shown to greatly red-shift with increasing aspect ratio.^[4] In addition, arrayed triangular nanoparticles of silver have been demonstrated as effective substrates for SERS in the spectral range from 700 to 800 nm, while spherical nanoparticles of silver are most suitable in the range of 530 to 570 nm.^[5] With regard to catalysis, cubic nanoparticles of platinum with surfaces enclosed by the {100} facets catalyze reactions involving hydrogen, while the reactivity of carbon monoxide is enhanced by the {210} facets of buckyball-shaped nanoparticles.^[6] In spite of its fundamental and technological importance (as well as a long history of study), the challenge to synthetically and systematically control the shape of metal nanostructures has been met with limited success. Design of a generic method for the preparation of metal nanostructures with a broad range of well-defined and controllable morphologies is still needed in order to fully exploit their peculiar properties and unique applications.

Recent studies have established that solution-phase methods have the potential to grow metal nanostructures in bulk quantities with a variety of well-defined morphologies. For silver and gold, nanorods and nanowires with controllable diameters and aspect ratios could be synthesized with soft templates, such as rod-shaped micelles self-assembled from cetyltrimethylammonium bromide (CTAB)^[7] or liquid crystalline phases made of sodium bis(2-ethylhexyl) sulfosuccinate (AOT), *p*-xylene, and water.^[8] Several types of planar, thin nanoplates of silver have been synthesized and studied since small silver nanospheres were first reported to be transformed into prismatic plates when subjected to irradiation by visible light.^[9] For example, a seed-mediated proto-

[a] B. Wiley, Dr. Y. Sun, Dr. B. Mayers, Prof. Y. Xia
Department of Chemistry
Department of Chemical Engineering
University of Washington, Seattle, Washington 98195 (USA)
Fax: (+1) 206-685-8665
E-mail: xia@chem.washington.edu

[⁺] These two authors contributed equally to this article.

col has been developed to generate truncated, triangular nanoplates and circular nanodisks of silver in the presence of CTAB micelles.^[10] Silver nanodisks have also been synthesized by sonicating AgNO₃ and hydrazine in the presence of reverse micelles self-assembled from an AOT/isooctane/water system.^[11] The octylamine/water bilayer system has been demonstrated as another soft template capable of producing silver nanoplates.^[12] In addition to surfactants, it was reported that the synthesis of silver nanoplates could be achieved by refluxing a solution of AgNO₃ in *N,N*-dimethyl formamide in the presence of a polymer, such as poly(vinyl pyrrolidone) (PVP).^[13] It is worth noting that polymer-mediated morphological evolution was also applicable to the synthesis of cubic and tetrahedral nanoparticles of platinum by reducing K₂PtCl₄ with H₂ gas in the presence of sodium polyacrylate.^[14] In general, each one of these approaches can generate only one or two shapes when the experimental parameters are changed. Here we focus on a polymer-mediated polyol process that allows for the preparation of silver nanostructures with a number of different well-controlled morphologies (e.g., cubes, rods, wires, and spheres) in large quantities by simply tuning the ratio between the capping agent (PVP) and the precursor salt (AgNO₃). It is also possible to generate thin nanoplates and nanobelts of silver by replacing PVP with another capping agent such as sodium citrate.

Polyol Synthesis: Past and Present

Polyol synthesis was originally developed by Fiévet and co-workers as a simple and versatile route to colloidal particles made of metals and alloys, with typical examples including Ag, Au, Cu, Co, Ir, Ni, Pd, Pt, Ru, CoNi, and FeNi.^[15] The primary reaction of this process involves the reduction of an inorganic salt (the precursor) by polyol at an elevated temperature. PVP is commonly added as a stabilizer to prevent agglomeration of the colloidal particles. Reasons for the popularity and versatility of this synthesis include the ability for polyols to dissolve (and solvate) many precursor salts (and ions), their highly temperature-dependent reducing power, and their relatively high boiling points (for ethylene glycol, it is about 196°C).^[16] In particular, the temperature-dependent reducing power of polyols makes them ideal for the synthesis of colloidal particles (usually quasi-spherical in shape) over a broad range of sizes, as it gives one the ability to control the nucleation and growth processes through careful regulation of reaction temperature. Furthermore, the use of solvents with high boiling points allows for the production of colloidal particles from some more reactive (and hence less reducible) metals such as Co, Ni, Cd, Bi, and Pb by thermally decomposing appropriate precursors.^[17]

The polyol process we have used for the silver work is mainly based on ethylene glycol, which serves as a good solvent for both AgNO₃ and PVP, because of its relatively high dielectric constant.^[18] At elevated temperatures, ethylene glycol can reduce Ag⁺ ions into Ag atoms, and thereby

induce the nucleation and growth of silver nanostructures in the solution phase. Our recent results suggest that PVP plays a critical role in producing silver nanostructures with good stability and size/shape uniformity.^[19] As revealed by infrared (IR) and X-ray photoelectron spectroscopy (XPS) studies, both the oxygen and nitrogen atoms of the pyrrolidone unit can promote the adsorption of PVP chains onto the surface of silver.^[20] This may explain why PVP has been successful as a capping agent (in addition to its role as a stabilizer), while many other polymers such as poly(ethylene oxide) and poly(vinyl alcohol) failed. Furthermore, it has been suggested that the interaction strengths between PVP and different crystallographic facets of a silver lattice were substantially different, and could therefore induce anisotropic growth for silver (a solid of highly isotropic in structure). Our recent experiments, in which small gold nanoparticles were attached as markers to the surfaces of silver nanowires through the dithiol linkage, verified that PVP interacted more strongly with silver atoms on the {100} facets than those on the {111} facets.^[21] This binding specificity can be attributed to the difference in surface atom density, 1.20×10^{19} versus $1.38 \times 10^{19} \text{ m}^{-2}$ for the {100} and {111} planes.

The experimental setup commonly employed in our work is shown in Figure 1. We have made a number of modifications to the conventional protocol developed by Fiévet et al.

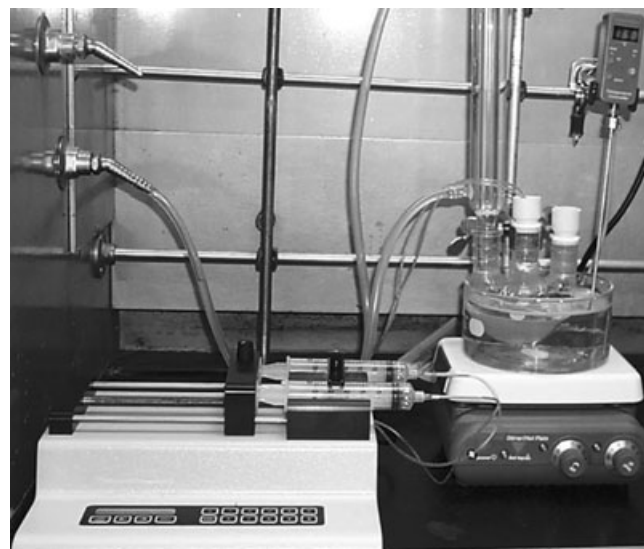


Figure 1. Setup for the synthesis of silver nanostructures via a polymer-mediated polyol process.

to achieve better control over the nucleation and growth steps. In a typical synthesis, anhydrous ethylene glycol (5 mL, 99.8%, Aldrich) was heated at 160°C for 1 h; then separate solutions of AgNO₃ (99+%, Aldrich) and PVP ($M_w \approx 55,000$, Aldrich) in ethylene glycol (each 3 mL) were simultaneously injected into the reaction flask by using a two-channel syringe pump at a rate of $375 \mu\text{L min}^{-1}$. The re-

duction of AgNO_3 by ethylene glycol at 160°C led to the formation of elemental silver (step I in Figure 2) at a moderate rate, because of the strong dependence of the reducing power of ethylene glycol on the reaction temperature.^[16] Clusters^[22] of a critical size (or nuclei) appeared (i.e., nucleation, steps II and III in Figure 2) once the concentration of zero-valent silver reached a critical value. This depiction is built upon LaMer's model for the nucleation of monodispersed sols in a homogeneous system.^[23] The hot solution consistently turned yellow as the AgNO_3 and PVP solutions were introduced, indicating the formation of silver nanoparticles with a roughly rounded profile, since such particles display a distinctive SPR peak around 400 nm.^[24] In the subsequent growth process (step IV in Figure 2), silver atoms generated from the reduction of AgNO_3 diffused to the surface of nuclei and positioned themselves at active surface sites, forming metallic bonds with their neighbors. By adjusting the molar ratio between PVP and AgNO_3 , the thickness of PVP coating and the location of PVP chains on the surface of a seed could both be modified. This modification, in turn, altered the resistance of each facet to growth (addition of silver atoms), and led to the formation of silver nanostructures with distinct shapes. The drawings on the right side of Figure 2 summarize three types of silver nanostructures that have been successfully synthesized by means of this PVP-mediated polyol process. Their growth mechanisms are discussed in the following sections.

Silver Nanocubes: Kinetically Controlled Growth

Perhaps the most intriguing morphology yet synthesized by this polyol process is the nanocube. To produce this type of nanostructure, the concentration of AgNO_3 in the final solution must be relatively high (0.125–0.25 M), and the molar ratio between PVP and AgNO_3 must be low (at ~ 1.5).^[19a] These conditions result in fast nucleation and growth of the silver seeds, and may therefore have reduced the time avail-

able for twin defects to form.^[25] In addition, since twinning is only favorable when the surface energy of the $\{100\}$ facets is greater than that of the $\{111\}$ facets,^[26] the presence of PVP can serve to reduce the driving force for twin formation through its selective interaction with the $\{100\}$ planes. Once a large proportion of single-crystal seeds form, selective adsorption of PVP on the $\{100\}$ facets will lead to preferential addition of silver atoms to the $\{111\}$ facets. As the growth rate in the $\langle 111 \rangle$ direction is greater than that in the $\langle 100 \rangle$ direction, the $\{100\}$ sides of the cube will become enlarged at the expense of the $\{111\}$ corners.^[27] After the cubic shape is formed, each face of the silver nanocube will have the same growth rate, and further growth will mainly increase the size with no significant morphological variation.

Figure 3 shows a combination of scanning electron microscopy (SEM) and transmission electron microscopy (TEM) images taken from silver nanocubes that were synthesized with the polyol method.^[19a] Figure 3A and B are SEM images of the product obtained at 45 min when the concentration of AgNO_3 was 0.25 M, indicating that this method could produce uniform silver nanocubes in high yields. The surfaces of these silver nanocubes are smooth, and their average edge length is 175 nm. Figure 3B also indicates that all corners and edges of these nanocubes are slightly truncated; the drawing in Figure 3C clearly delineates these truncations and their corresponding crystallographic planes. Figure 3C shows the X-ray diffraction (XRD) pattern recorded from the same batch of silver nanocubes, with all peaks assigned to diffraction from the (111) , (200) , and (220) planes of silver, respectively. It is worth noting that the ratio between the intensities of the (200) and (111) diffraction peaks in this XRD pattern is 0.67, which is 68% greater than the value obtained from a conventional powder sample (Joint Committee on Powder Diffraction Standards file no. 04-0783). This result indicates that, because the sides of the cubes are bound by enlarged $\{100\}$ facets, the $\{100\}$ planes of silver are preferentially oriented parallel to the substrate, as is confirmed by the TEM and SEM images.

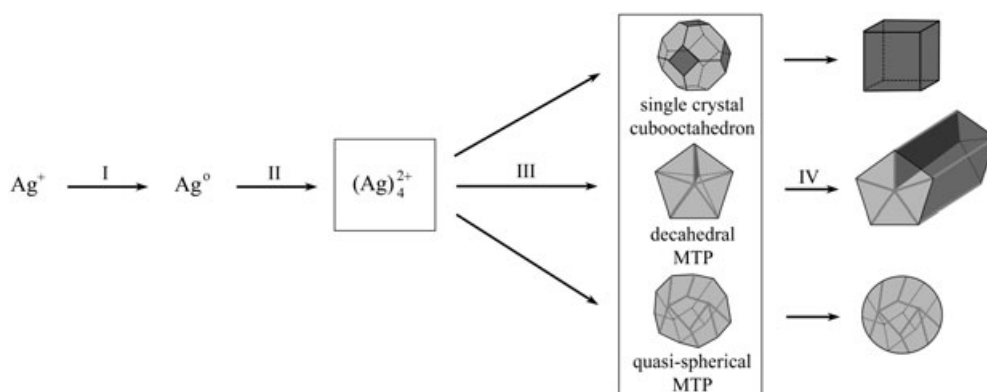


Figure 2. Schematic illustrating the reduction of silver ions by ethylene glycol (I); the formation of silver clusters (II); the nucleation of seeds (III); and the growth of seeds into nanocubes, nanorods or nanowires, and nanospheres (IV). The formation of metal clusters and seeds with different crystallinities depicted in the boxes is currently being studied. This article focuses on the growth of silver nanostructures with well-defined and controllable shapes. The surfaces marked in light and dark gray represent the $\{111\}$ and $\{100\}$ facets, respectively. The light gray lines and dark gray interior planes represent the twinned boundaries and twinned planes, respectively.

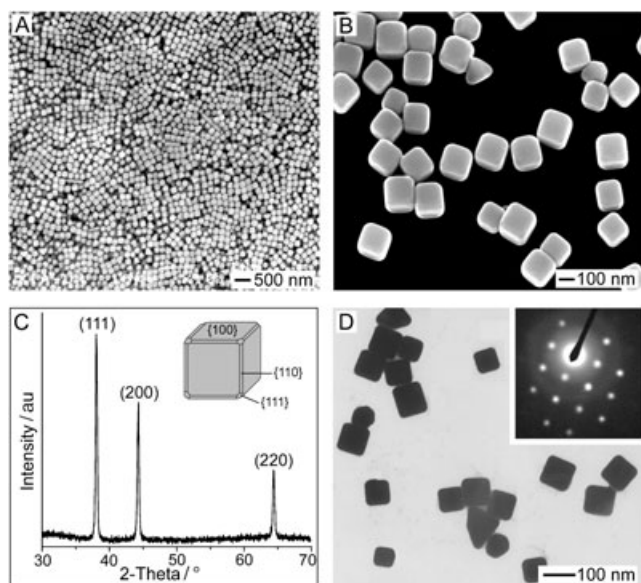


Figure 3. A,B) SEM images of silver nanocubes that were synthesized by heating the mixture of AgNO_3 and PVP in ethylene glycol for 45 min. The sample stage was tilted at 20° in B, showing that all the corners and edges of each cube were slightly truncated. C) XRD pattern obtained from the same batch of nanocubes deposited on a glass substrate. The drawing of one cube is shown as the inset. In this synthesis, the concentration of AgNO_3 solution was 0.25 M and the molar ratio between PVP and AgNO_3 was 1.5. D) A TEM image of the product obtained under the same conditions as in A, except that the concentration of AgNO_3 was reduced to 0.125 M and the growth time was shortened to 30 min. The inset shows a typical electron diffraction pattern taken from any individual nanocube by directing the electron beam perpendicular to one of its square faces.

The ratio between the intensities of the (220) and (111) peaks is also slightly higher than usual (0.33 versus 0.25), because of the relative abundance of {110} facets on the truncated edges of the silver nanocubes.

The size of the silver nanocubes can be varied by changing the concentration of AgNO_3 . Figure 3D shows a TEM image of silver nanocubes that were synthesized by decreasing the AgNO_3 concentration from 0.25 to 0.125 M and shortening the growth time from 45 to 30 min. These adjustments reduced their average edge length from 175 to 80 nm. The inset is a typical electron diffraction pattern recorded by directing the electron beam perpendicular to one of the square faces of an individual cube. The exactly square symmetry of this pattern confirms that each silver nanocube was a single crystal bound primarily by {100} facets.

Silver Nanowires: Twin-Induced Growth

To alter the polyol process so that silver nanowires (rather than nanocubes) are produced in high yields, one only needs to reduce the concentration of AgNO_3 while keeping the ratio between PVP and AgNO_3 unchanged. It is known that, by lowering precursor concentration, one reduces the chemical potential (i.e., driving force) for crystallization.^[28] It has

also been theoretically demonstrated that the multiply twinned decahedra is the most thermodynamically stable seed, as it is bound almost entirely by the lower energy {111} facets.^[25] Thus, by lowering precursor concentration, it is possible to decrease the chemical potential to a sufficiently low level so that multiple-twinned particles (MTPs, thermodynamically more stable, often in the decahedral shape), rather than single-crystal seeds (kinetically stable) will be formed. Since the twin defect represents the highest energy site on the surface of an MTP, silver atoms will preferentially crystallize on those sites, leading to uniaxial elongation of the decahedra into a pentagonal rod, whose sides are bound by {100} facets (see Figure 2). Once the pentagonal rod has formed, PVP will interact more strongly with the {100} sides than with the {111} ends. Therefore, the nanorod can readily grow into a longer wire, because its side surfaces are tightly passivated by PVP, while its ends remain reactive toward the arriving silver atoms. As a result, the pentagonal cross section, the straightness of the five side edges, and the flatness of the side surfaces can all be retained as the nanorods grow into nanowires as long as hundreds of micrometers.

Figure 4A shows a typical SEM image of silver nanowires that were prepared with an AgNO_3 concentration of 0.085 M.

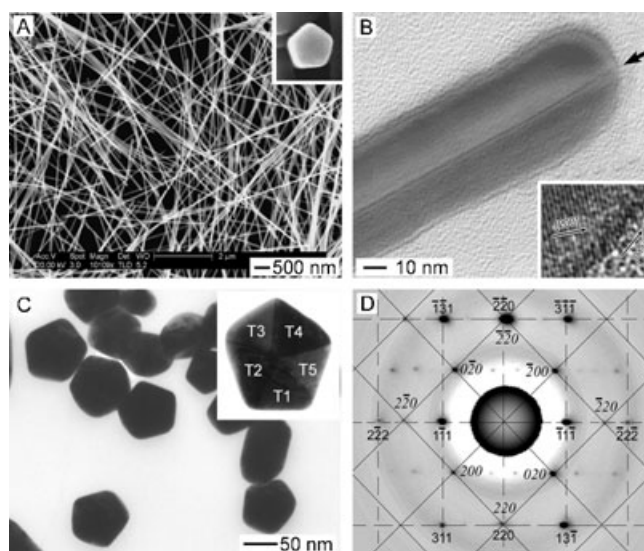


Figure 4. A) SEM image of silver nanowires, demonstrating their uniformity in diameter (~ 50 nm) along the entire nanowire length. The inset is an SEM image taken from the cross section of a broken nanowire. B) TEM image taken from the end of an individual nanowire, showing the existence of a twin plane along its longitudinal axis (as indicated by the arrow). The inset in the lower right shows a HRTEM image taken from the side of a nanowire. C) TEM image of a microtomed sample of nanowires shown in A, indicating the pentagonal symmetry of their cross sections. The inset in C is a TEM image with slightly higher magnification that was taken from an individual Ag nanowire, confirming that each wire had a fivefold twinned structure characterized by five single-crystal subunits. D) SAED pattern taken from an individual nanowire by aligning the electron beam perpendicular to one of the five side surfaces (e.g., the side surface of subunit T1). In this synthesis, the molar ratio between PVP and AgNO_3 was 1.5 and the concentration of AgNO_3 was 0.085 M.

The inset gives an image of a nanowire intentionally broken by sonication for 1 h, clearly showing its pentagonal cross section and flat edges. Figure 4B shows a TEM image taken from an individual nanowire, making evident the existence of a twin plane along the longitudinal axis. Note that no matter which side of the nanowire lay against the surface of the TEM grid, the geometry of the wire guarantees that a twin boundary will always appear to be in the middle of the wire. The inset at the bottom-right corner is a high-resolution TEM (HRTEM) image taken from the side of a nanowire, providing evidence for the single crystallinity in each of its five domains. This inset also demonstrates that growth of this wire occurred in the $[01\bar{1}]$ direction.

To further study the crystallographic nature of the silver nanowires, a sample of nanowires was microtomed and examined under TEM (Figure 4C). As expected, most of the cross sections shown in this image are pentagonal in shape. The nonpentagonal cross sections can be attributed to two causes: 1) random orientations of the wires relative to the edge of the microtome knife, and 2) co-existence of a small amount of silver particles in this sample. The inset gives the TEM image of a pentagonal cross section (at a slightly higher magnification), clearly disclosing the fivefold contrast resulting from the differences in crystal orientation induced by the twin defects. The stark contrast across each twin plane implies that each silver nanowire contained five single-crystal subunits, which are marked as T1, T2, T3, T4, and T5.

Since each silver nanowire is an assembly of five subunits separated by $\{111\}$ twin planes, its electron diffraction pattern is more complex than a single-crystal silver nanostructure. Figure 4D gives the typical selected-area electron diffraction (SAED) pattern recorded from an individual nanowire by aligning the electron beam perpendicular to one of the five sides (e.g., the electron beam was perpendicular to the side surface of subunit T1 in the inset of Figure 4C). The indexed results indicate that this pattern contained an interpenetrated set of two different diffraction patterns. The one with square symmetry (marked with solid lines) corresponds to the $[001]$ zone axis of T1; the one with rectangular symmetry (marked with dashed lines) corresponds to the $[1\bar{1}\bar{2}]$ and $[\bar{1}1\bar{2}]$ zone axes of T3 and T4, respectively. The mutual orientation of these two zones causes double diffraction, resulting in the generation of the remaining spots. Subunits T2 and T5 did not contribute to the diffraction pattern as they were not in an observable Bragg diffraction orientation. These assignments are consistent with the results obtained for multiply twinned nanorods of gold and copper with the same pentagonal symmetry and $\{100\}$ side surfaces.^[29] While nanorods of these coinage metals were synthesized under quite different conditions, the fact that all of them follow a similar growth mechanism leads us to believe that a polymer-mediated polyol process should be extendable to the synthesis of nanowires for metals other than silver.

Silver Nanospheres: Isotropic Growth

Nanoparticles with quasi-spherical shapes have conventionally been obtained when the molar ratio between PVP and AgNO_3 was relatively high (>5).^[30] In this case, any surface specific adsorption is overwhelmed and the entire surface of the initially formed seeds is covered with a thick coating of PVP (as indicated in the inset of Figure 5). As the resistance

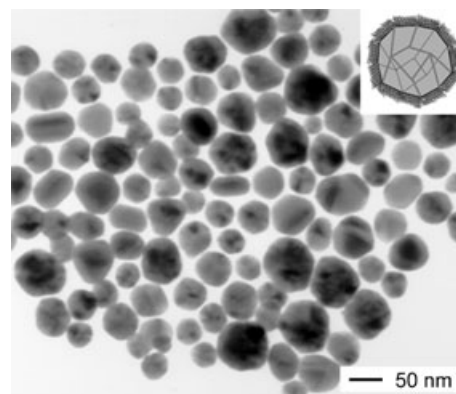


Figure 5. TEM images of silver nanoparticles formed when the molar ratio between PVP and AgNO_3 was 15 and the concentration of AgNO_3 was 0.25 M. The inset illustrates the thick, isotropic coating of PVP that might be present on the surface of silver particles involved in this synthesis.

to surface addition by the silver atoms is now nearly isotropic, growth of the seeds proceeds in an isotropic manner as well. Figure 5 shows the TEM image of a typical product that was prepared when the ratio between PVP and AgNO_3 was 15 in the reaction mixture. These particles are essentially spherical in shape although a few slightly anisotropic particles can be observed. The formation of anisotropic colloids might be ascribed to preferential addition of silver atoms at the high-energy twin sites, resulting in the formation of relatively short rods, or to the geometric limitations imposed by the faceted nature of the silver crystal. It is not clear whether the surfaces of the anisotropic nanoparticles were bound by $\{111\}$ facets, $\{100\}$ facets, or a combination of them.

Silver Nanoplates and Nanobelts: Citrate versus PVP

To produce nanostructures bound primarily by $\{111\}$ facets, it is evident that a capping agent other than PVP must be employed. Recently we and other groups have found that sodium citrate can promote the formation of triangular nanoplates and nanobelts of silver bound mainly by the $\{111\}$ planes.^[31] In a typical procedure, small silver nanospheres were first synthesized in an aqueous solution by reducing AgNO_3 with NaBH_4 in the presence of PVP and sodium citrate at room temperature. A TEM image of these initial nanoparticles is shown in Figure 6A. The average diameter of these nanoparticles is ~ 3.5 nm. When this disper-

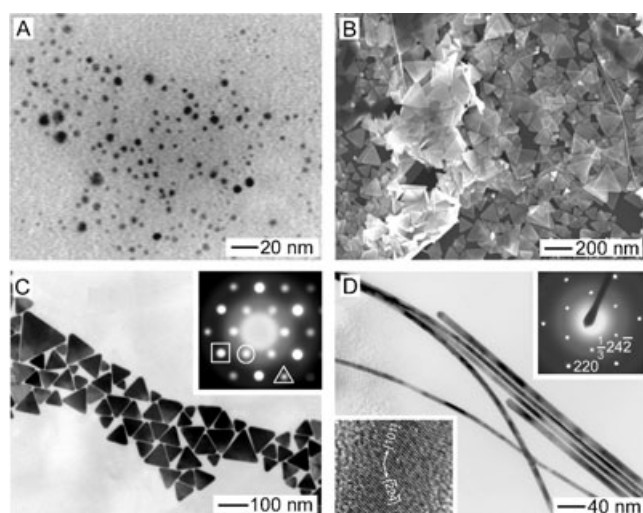


Figure 6. A) TEM image of the initial silver nanoparticles with diameter of ~ 3.5 nm. B) SEM image of the product that was obtained by refluxing these small silver nanospheres in the presence of PVP and sodium citrate, showing the formation of a mixture of triangular nanoplates (with sharp corners) and nanobelts of silver. Some nanoplates were oriented with their triangular faces perpendicular to the supporting substrate. C) A TEM image of triangular nanoplates self-assembled into a stripe of monolayer, clearly indicating the bimodal sizes of nanoplates. The inset gives a typical electron microdiffraction pattern taken from an individual nanoplate supported on the TEM grid against one of its triangular faces. D) A TEM image of silver nanobelts whose flat faces were oriented parallel to the surface of the supporting substrate. The inset in the lower left demonstrates the nanobelts were single crystals, and grew along the $[101]$ direction. The other inset shows a typical SAED pattern taken from an individual nanobelt.

sion was refluxed under ambient conditions for 10 h, the silver nanospheres were transformed into a mixture of triangular nanoplates (95%) and nanobelts (5%) through a process such as Ostwald ripening. An SEM image of this mixture is shown in Figure 6B. Note that the triangular nanoplates have sharp corners, and, as can be seen by observing those plates whose triangular faces were oriented perpendicular to the substrate, they are thin and flat. Due to their flat surfaces, sharp corners, smooth edges, and shape regularity, these silver nanoplates tend to assemble into a monolayer on the surface of a carbon-coated TEM grid (as shown in Figure 6C). The inset shows the electron microdiffraction pattern obtained when the electron beam was directed perpendicular to the triangular face of an individual plate, suggesting that each plate was a single crystal. The strongest intensity spot (see the square) corresponds to Bragg diffraction from the $\{220\}$ lattice planes of silver, proving that the triangular faces of the nanoplates are composed of $\{111\}$ planes. The outer spots (see the triangle) correspond to reflection from the $\{422\}$ planes, while the inner spots (circle) could be ascribed to the $(1/3)\{422\}$ reflection. It is worth pointing out that this last reflection is only observable from atomically flat surfaces of silver (or gold).^[32]

The silver nanobelts could be separated from the mixture by centrifugation. TEM images (Figure 6D) of these nanostructures reveal that they are uniform in both lateral di-

mension (~ 9 nm) and surface smoothness, with lengths up to $25 \mu\text{m}$. A selected area electron diffraction (SAED) pattern taken from a single nanobelt (see inset) displays the same $(1/3)\{422\}$ reflection as that seen for a nanoplate, suggesting that these nanostructures are also composed of atomically smooth and flat facets. The $\{220\}$ reflection confirms that the wider side surfaces of the belts are composed of $\{111\}$ planes. The lower left inset is a typical HRTEM image of a nanobelt, indicating that growth of this single-crystal nanobelt occurs along the $[101]$ axis.

In a related study, we also found that visible light alone could induce the morphological transformation of silver nanospheres into triangular nanoplates in the presence of PVP and citrate at room temperature.^[33] To separate the roles of PVP and citrate, these two chemicals were added at different stages of the synthetic process. First, silver nanospheres with a mean diameter of 4.3 nm were obtained by using only PVP as the stabilizer during the reduction by NaBH_4 . When this dispersion was subjected to irradiation with visible light, no morphological change was observed. However, if citrate was added to the PVP-stabilized dispersion before irradiation, the spherical particles were transformed into triangular nanoplates. These experiments established that citrate was the key component in this morphological transformation from spheres into thin plates bounded by $\{111\}$ facets. If the initial reduction by NaBH_4 was performed in the presence of sodium citrate only, relatively large particles (10–20 nm) were obtained due to agglomeration. Such nanoparticles could not be transformed into other shapes. Therefore, it seems to be that the primary role of PVP in this process is to stabilize silver nanospheres with diameters (< 10 nm) less than the critical size required for morphological transformation.

Optical Properties of Silver Nanostructures

The sensitive dependence of SPR peak position on the exact morphology of metal nanostructures has been theoretically predicted for some time.^[34] However, their relationship has not been rigorously investigated experimentally due to the difficulties in obtaining particles with well-defined shapes in bulk quantities. The silver nanostructures synthesized by means of the PVP-mediated polyol process provide an avenue to systematically study the correlation between the SPR feature and the particle morphology. Figure 7 shows the UV-visible extinction spectra of three aqueous dispersions that contained silver spheres, cubes, and triangular thin plates with roughly the same lateral dimensions (~ 80 nm). The silver nanospheres exhibited one symmetric extinction peak centered at 430 nm. However, cubic nanoparticles displayed three SPR peaks located at 350, 400, and 470 nm, respectively. In general, the number of SPR peaks increased as the symmetry of particles decreased: spherical particles (with C_s symmetry) have only one peak, whereas three peaks are often observed for cubic ones (with O_h symmetry).^[35]

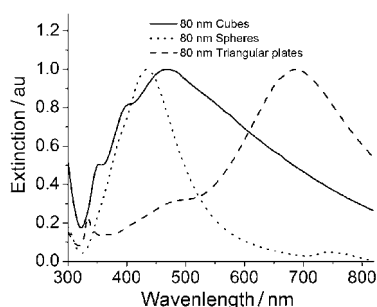


Figure 7. UV-visible/near-infrared spectra recorded from aqueous dispersions containing quasi-spheres, cubes, and triangular thin plates of silver with roughly the same lateral dimensions. Note that both the number of SPR modes and their positions change as the shape varies. The spectra have been normalized against the intensities of their strongest peaks.

The extinction spectra of the triangular nanoplates displayed three peaks at 335, 470, and 690 nm. Theoretical calculations by Schatz and co-workers attribute these peaks to the out-of-plane quadrupole, in-plane quadrupole, and in-plane dipole plasmon resonance modes, respectively.^[36] The triangular silver nanoplates with slightly truncated corners produced by the photoinduced process displayed a blue-shift for the peak around 690 nm.^[33] This observation agreed with Schatz's theoretical prediction that the in-plane dipole resonance mode was highly sensitive to the sharpness of the corners. The unique SPR features of these silver nanoparticles should make them particularly useful in applications such as sensing, plasmonics, and biological imaging.^[37]

In addition to their interesting far-field optical properties, silver nanoparticles exhibit very large local electromagnetic fields when illuminated by light with wavelengths corresponding to their SPR peaks. These enhanced near fields play a key role in SERS, in which the Raman spectrum of a molecule near the surface of a nanoparticle can be enhanced by several orders of magnitude.^[38] Nanoparticles with sharp corners or edges (e.g., pentagonal nanowires, cubes, triangular plates) are especially active SERS substrates, as local values of $|E|^2$ can be more than 500 times that of the applied field.^[36] This corresponds to a Raman enhancement of 10^5 at a distance 1 nm from the particle surface. Since near field plasmon peaks can also be tuned by changing the shape of a nanostructure, the polyol synthesis described in this article may provide a powerful route to ideal SERS substrates. By fine-tuning the properties of silver nanostructures, it might be feasible to make single-molecule detection the new standard for the Raman spectroscopic technique.^[39]

Metal Nanostructures with Hollow Interiors

The ability to control the SPR features of silver nanostructures can be further extended through their transformation into hollow nanostructures by using a template-engaged process.^[40] To this end, we have demonstrated the use of the galvanic replacement reaction between silver and HAuCl_4 as a simple and versatile route to nanostructures of gold and

Au/Ag alloys with hollow interiors and highly crystalline walls.^[19a] In this synthesis, the silver nanostructure serves as both a source of electrons and physical template, around which gold atoms are generated through a redox process. The resultant structure has a morphology complementary to that of the silver template, with the interior void mainly determined by the size of the template. Such a template-engaged process has been successfully applied to a number of noble metals such as Au, Pd, and Pt. The details of the morphological, compositional, structural, and spectral changes involved in the entire process have been elucidated to some extent.^[41] Our most recent study of the Ag/HAuCl_4 system implies that the templating process proceeds through at least two distinct steps:^[42] 1) the formation of pinhole-free shells with homogeneous, uniform walls consisting of Au/Ag alloy through a combination of galvanic replacement reaction, alloying, and possibly Ostwald ripening; and 2) the development of pores in the shells (to form cages) through dealloying, in which silver atoms are selectively extracted from the alloyed walls. As alloying and dealloying proceed, the SPR peaks of resultant hollow and/or porous nanostructures can be conveniently tuned in the spectral region from visible to near infrared. Taking silver nanocubes as an example (see Figure 8), titration with increasing amounts of

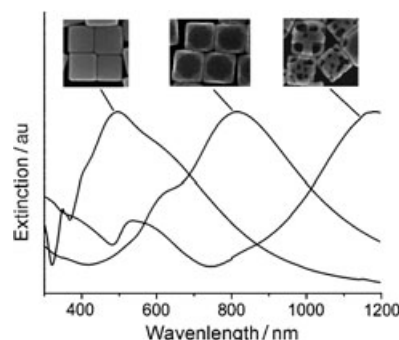


Figure 8. UV-visible/near-infrared spectra of an aqueous dispersion of silver nanocubes before and after different volumes of an aqueous HAuCl_4 solution (1 M^{-3}) were added: 0.00, 1.00, and 2.25 mL. The spectra have been normalized against the intensities of their strongest peaks. Note that the major extinction peak was continuously shifted towards the near infrared region as more HAuCl_4 was used to titrate the silver nanocubes. The insets are the SEM images of nanoparticles contained in the corresponding samples (from left to right): nanocubes of silver ($\sim 111 \text{ nm}$ in edge length), nanoboxes of a silver/gold alloy, and nanocages (porous nanoboxes) of gold.

HAuCl_4 resulted in the formation of gold hollow nanostructures (without and with porous walls) whose SPR peaks could be continuously swept from 495 nm to 1180 nm.

Perspective Conclusion

Shape-controlled synthesis of metal nanostructures has the potential to provide us with an unprecedented level of control over both nanoscale and bulk material properties. We

have demonstrated that the PVP-mediated polyol process is capable of producing silver nanostructures with a number of well-defined shapes that include cube, rod/wire, and sphere. In each case, the formation of a distinct morphology is determined by the crystallinity or twin structure of the initial seeds, the selective interaction between the capping agent (in this case, PVP) and different crystallographic planes of silver, and the level of surface coverage provided by PVP. These parameters could be controlled, to some extent, by varying the concentration of AgNO_3 (a precursor to elemental silver), as well as the molar ratio between PVP and AgNO_3 . Through incorporation of other capping agents (e.g., sodium citrate), it was shown that enlargement of the {111} rather than {100} planes of silver could also be promoted, resulting in the formation of triangular nanoplates and nanobelts enclosed mainly by {111} facets.

While the growth mechanism for each nanostructure has been explained in detail, we can still only hypothesize on what factors control the crystallinity or twin structure of seeds involved in the nucleation stage. Understanding the process of seed formation is critical, as it seems the number of twin planes in the initial seed is the key factor for determining the shape exhibited by the final product (e.g., single-crystal seeds form cubes, multiply-twinned decahedral seeds form wires, etc). A systematic study of the nucleation and seed formation steps is currently underway in our group. Achieving greater control over these stages of nanostructure formation may open avenues to new shapes and higher yields.

As the polyol synthesis has already been developed to produce colloidal particles from a large number of metals, there is no reason why nanostructures with well-defined shapes cannot be obtained from these metals as well. Copper, gold, palladium, and platinum are some particularly good candidates, as they all crystallize in a face-centered cubic structure similar to that of silver, and hence the selectivity in interaction between the capping agent and various crystallographic planes may share the same mechanism. Indeed, polyol synthesis of gold nanostructures with well-defined shapes has recently been demonstrated by Yang and his co-workers.^[43] Single-crystal nanowires of platinum have been synthesized by our group by using a polyol process, with PVP as the capping agent.^[44] Although different capping agents may be required, it is believed that the level of shape-control that has been realized for silver should be achievable for other metals as well.

Acknowledgement

This work has been supported in part by a grant from the ONR (N-00014-01-1-0976), a DARPA-DURINT subcontract from Harvard University, a Career Award from the NSF (DMR-9983893), and a Fellowship from the David and Lucile Packard Foundation. Y.X. is a Camille Dreyfus Teacher Scholar (2002) and an Alfred P. Sloan Research Fellow (2000). B.W. and B.M. have been supported by two IGERT fellowships (funded by NSF, DGE-9987620) from the Center for Nanotechnology at the UW.

- [1] a) W. P. Halperin, *Rev. Mod. Phys.* **1996**, *58*, 533; b) G. Schmid, *Chem. Rev.* **1992**, *92*, 1709; c) A. Henglein *Chem. Rev.* **1989**, *89*, 1861; d) L. N. Lewis, *Chem. Rev.* **1993**, *93*, 2693; e) G. Schön, U. Simon, *Colloid Polym. Sci.* **1995**, *273*, 101; f) G. Schmidt, L. F. Chi, *Adv. Mater.* **1998**, *10*, 515; g) R. D. Theys, G. Sosnovsky, *Chem. Rev.* **1997**, *97*, 83; h) S. A. Maier, M. L. Brongersma, P. G. Kik, S. Meltzer, A. A. G. Requicha, H. A. Atwater, *Adv. Mater.* **2001**, *13*, 1501; i) P. V. Kamat, *J. Phys. Chem. B* **2002**, *106*, 7729; j) C. B. Murray, S. Sun, H. Doyle, T. Betley, *MRS Bull.* **2001**, *26*, 985; k) M.-P. Pileni, *Adv. Funct. Mater.* **2001**, *11*, 323; l) M. D. Malinsky, K. L. Kelly, G. C. Schatz, R. P. van Duyne, *J. Am. Chem. Soc.* **2001**, *123*, 1471.
- [2] a) U. Kreibitz, M. Vollmer, *Optical Properties of Metal Clusters*, Springer, New York, **1995**; b) M. A. El-Sayed, *Acc. Chem. Res.* **2001**, *34*, 257; c) J. B. Jackson, N. J. Halas, *J. Phys. Chem. B* **2001**, *105*, 2473; d) S. L. Westcott, S. J. Oldenburg, T. R. Lee, N. J. Halas, *Chem. Phys. Lett.* **1999**, *300*, 651.
- [3] a) T. R. Jensen, L. Kelly, A. Lazarides, G. C. Schatz, *J. Cluster Sci.* **1999**, *10*, 295; b) J. P. Kottmann, O. J. F. Martin, D. R. Smith, S. Schultz, *Phys. Rev. B* **2001**, *64*, 235402; c) I. O. Sosa, C. Noguez, R. G. Barrera, *J. Phys. Chem. B* **2003**, *107*, 6269.
- [4] a) C. J. Murphy, N. R. Jana, *Adv. Mater.* **2002**, *14*, 80; b) F. Kim, J. H. Song, P. Yang, *J. Am. Chem. Soc.* **2002**, *124*, 14316.
- [5] a) L. A. Dick, A. D. McFarland, C. L. Haynes, R. P. Van Duyne, *J. Phys. Chem. B* **2002**, *106*, 853; b) M. Muniz-Miranda, *Chem. Phys. Lett.* **2001**, *340*, 437.
- [6] a) A.-C. Shi, R. I. Masel, *J. Catal.* **1989**, *120*, 421; b) L. M. Falicov, G. A. Somorjai, *Proc. Natl. Acad. Sci. USA* **1985**, *82*, 2207.
- [7] a) N. R. Jana, L. Gearheart, C. J. Murphy, *Adv. Mater.* **2001**, *13*, 1389; b) N. R. Jana, L. Gearheart, C. J. Murphy, *J. Phys. Chem. B* **2001**, *105*, 4065; c) Y.-Y. Yu, S.-S. Chang, C.-L. Lee, C. R. C. Wang, *J. Phys. Chem. B* **1997**, *101*, 6661.
- [8] L. M. Huang, H. T. Wang, Z. B. Wang, A. Mitra, K. N. Bozhilov, Y. S. Yan, *Adv. Mater.* **2002**, *14*, 61.
- [9] a) R. Jin, Y. Cao, C. A. Mirkin, K. L. Kelly, G. C. Schatz, J. G. Zheng, *Science* **2001**, *294*, 1901; b) R. Jin, Y. C. Cao, E. Hao, G. S. Metraux, G. C. Schatz, C. A. Mirkin, *Nature* **2003**, *425*, 487.
- [10] a) S. Chen, D. L. Carroll, *Nano Lett.* **2002**, *2*, 1003; b) S. Chen, Z. Fan, D. L. Carroll, *J. Phys. Chem. B* **2002**, *106*, 10777.
- [11] M. Maillard, S. Giorgio, M.-P. Pileni, *Adv. Mater.* **2002**, *14*, 1084.
- [12] D. O. Yener, J. Sindel, C. A. Randall, J. H. Adair, *Langmuir* **2002**, *18*, 8692.
- [13] I. Pastoriza-Santos, L. M. Liz-Marzán, *Nano Lett.* **2002**, *2*, 903.
- [14] T. S. Ahmadi, Z. L. Wang, T. C. Green, A. Henglein, M. A. El-Sayed, *Science* **1996**, *272*, 1924.
- [15] a) F. Fiévet, J. P. Lagier, M. Figlarz, *MRS Bull.* **1989**, *14*, 29; b) F. Fievet, J. P. Lagier, B. Blin, B. Beaudoin, M. Figlarz, *Solid State Ionics* **1989**, *32/33*, 198; c) G. Viau, F. Fiévet-Vincent, F. Fiévet, *Solid State Ionics* **1996**, *84*, 259; d) P. Toneguzzo, G. Viau, O. Acher, F. Fiévet-Vincent, F. Fiévet, *Adv. Mater.* **1998**, *10*, 1032; e) F. Bonet, V. Delmas, S. Grugeon, R. H. Urbina, P. Y. Silvert, K. Tekaiia-Elhissien, *Nanostr. Mater.* **1999**, *11*, 1277.
- [16] C. Ducamp-Sanguesa, R. Herrera-Urbina, M. Figlarz, *J. Solid State Chem.* **1992**, *100*, 272.
- [17] a) M. Figlarz, F. Fiévet, J. P. Lagier, Reduction of Metal Compounds to Metal Powders by Polyols. US Patent 4539041, Dec 20, **1983**; b) Y. Wang, T. Herricks, Y. Xia, *Nano Lett.* **2003**, *3*, 1163; c) Y. Wang, X. Jiang, T. Herricks, Y. Xia, *J. Phys. Chem. B* **2004**, *108*, 8641; d) Y. Wang, Y. Xia, *Nano Lett.* **2004**, *10*, 2047.
- [18] W. S. Jones, W. S. Tamplin in *Glycols* (Eds.: G. O. Curme, Jr., F. Johnston), Reinhold, New York, **1952** p. 38.
- [19] a) Y. Sun, Y. Xia, *Science* **2002**, *298*, 2176; b) Y. Sun, Y. Xia, *Adv. Mater.* **2002**, *14*, 833; c) Y. Sun, B. Gates, B. Mayers, Y. Xia, *Nano Lett.* **2002**, *2*, 165; d) Y. Sun, Y. Yin, B. Mayers, T. Herricks, Y. Xia, *Chem. Mater.* **2002**, *14*, 4736.
- [20] a) F. Bonet, K. Tekaiia-Elhissien, K. V. Sarathy, *Bull. Mater. Sci.* **2000**, *23*, 165; b) Z. Zhang, B. Zhao, L. Hu, *J. Solid State Chem.* **1996**, *121*, 105; c) H. H. Huang, X. P. Ni, G. L. Loy, C. H. Chew, K. L. Tan, F. C. Loh, J. F. Deng, G. Q. Xu, *Langmuir* **1996**, *12*, 909.

- [21] Y. Sun, B. Mayers, T. Herricks, Y. Xia, *Nano Lett.* **2003**, 3, 955.
- [22] A. Heinglein, *J. Phys. Chem.* **1993**, 97, 5457.
- [23] V. K. LaMer, R. H. Dinegar, *J. Am. Chem. Soc.* **1950**, 72, 4847.
- [24] S. M. Heard, F. Grieser, C. G. Barraclough, *J. Colloid Interface Sci.* **1983**, 93, 545.
- [25] a) L. D. Marks, *Rep. Prog. Phys.* **1994**, 57, 603; b) C. Cleveland, U. Landman, *J. Chem. Phys.* **1991**, 94, 7376.
- [26] J. Dundurs, L. D. Marks, P. M. Ajayan, *Philos. Mag. A* **1988**, 57, 605.
- [27] Z. L. Wang, *J. Phys. Chem. B* **2000**, 104, 1153.
- [28] J. W. Mullin, *Crystallization*, 3rd ed., Oxford, **1997**.
- [29] a) C. J. Johnson, E. Dujardin, S. A. Davis, C. J. Murphy, S. Mann, *J. Mater. Chem.* **2002**, 12, 1765; b) I. Lisiecki, A. Filankembo, H. Sack-Kongehl, K. Weiss, M.-P. Pileni, J. Urban, *Phys. Rev. B* **2000**, 61, 4968.
- [30] P.-Y. Silvert, R. Herrera-Urbona, N. Duvauchelle, V. Vijayakrishnan, K. T. Elhsissen, *J. Mater. Chem.* **1996**, 6, 573.
- [31] Y. Sun, B. Mayers, Y. Xia, *Nano Lett.* **2003**, 3, 675.
- [32] J. G. Allpress, J. V. Sanders, *Surf. Sci.* **1967**, 7, 1.
- [33] Y. Sun, Y. Xia, *Adv. Mater.* **2003**, 15, 695.
- [34] a) R. Gans, *Ann. Phys.*, **1915**, 47, 270; b) G. C. Papavassiliou, *Prog. Solid State Chem.* **1980**, 12, 185; c) *Light Scattering by Nonspherical Particles* (Eds.: M. I. Mishchenko, J. W. Hovenier, L. D. Travis), Academic Press, San Diego, **2000**.
- [35] D. E. Sands, *Introduction to Crystallography*, Dover, New York, **1993**, p. 51.
- [36] K. L. Kelly, E. Coronado, L. L. Zhao, G. C. Schatz, *J. Phys. Chem. B* **2003**, 107, 668.
- [37] a) A. D. McFarland, R. P. Van Duyne, *Nano Lett.* **2003**, 3, 1057; b) L. Hirsch, R. Stafford, J. Bankson, S. Sershen, B. Rivera, R. Price, J. D. Hazle, N. Halas, J. West, *Proc. Natl. Acad. Sci. USA* **2003**, 100, 13549; c) Y. Sun, Y. Xia, *Anal. Chem.* **2002**, 74, 5297.
- [38] a) H. Metiu, *Prog. Surf. Sci.* **1984**, 17, 153; b) M. Moskovits, *Rev. Mod. Phys.* **1985**, 57, 783; c) G. C. Schatz, *Acc. Chem. Res.* **1984**, 17, 370.
- [39] a) K. Kneipp, Y. Wang, H. Kneipp, L. T. Perelman, I. Itzkan, R. R. Dasari, M. S. Feld, *Phys. Rev. Lett.* **1997**, 78, 1667; b) S. Nie, S. R. Emory, *Science* **1997**, 275, 1102.
- [40] a) Y. Sun, B. T. Mayers, Y. Xia, *Nano Lett.* **2002**, 2, 481; b) Y. Sun, B. Mayers, Y. Xia, *Adv. Mater.* **2003**, 15, 641.
- [41] a) G. S. Metraux, Y. Cao, R. Jin, C. A. Mirkin, *Nano Lett.* **2003**, 3, 519; b) E. Hao, S. Y. Li, R. C. Bailey, S. L. Zou, G. C. Schatz, J. T. Hupp, *J. Phys. Chem. B* **2004**, 108, 1224.
- [42] Y. Sun, Y. Xia, *J. Am. Chem. Soc.* **2004**, 126, 3892.
- [43] F. Kim, S. Connor, H. Song, T. Kuykendall, P. Yang, *Angew. Chem.* **2004**, 116, 3759; *Angew. Chem. Int. Ed.* **2004**, 43, 3673.
- [44] J. Chen, T. Herricks, M. Geissler, Y. Xia, *J. Am. Chem. Soc.* **2004**, 126, 10854.

Published online: November 25, 2004